Detection and localization of Goliath grouper using their low-frequency pulse sounds

Ali Salem Altaher, Hanqi Zhuang, Ali K. Ibrahim, et al.

ARTICLES YOU MAY BE INTERESTED IN

CALL FOR PAPERS

JASA
THE JOURNAL OF THE
ACOUSTICAL SOCIETY OF AMERICA

Special Issue: Fish Bioacoustics:
Hearing and Sound Communication

ARTICLE

Detection and localization of Goliath grouper using their low-frequency pulse sounds

Ali Salem Altaher,[1,a),b)] (iD) Hanqi Zhuang,[1] Ali K. Ibrahim,[1,b)] Ali Muhamed Ali,[1,b)] Ahmed Altaher,[1,b)]
James Locascio,[2] Michael P. McCallister,[3] Matthew J. Ajemian,[3] and Laurent M. Chérubin[3]

[1]*Electrical Engineering and Computer Science Department, Florida Atlantic University, Boca Raton, Florida 33431, USA*

[2]*Mote Marine Laboratory, Sarasota, Florida 34236, USA*

[3]*Harbor Branch Oceanographic Institute, Florida Atlantic University, Fort Pierce, Florida 34946, USA*

ABSTRACT:

The goal of this paper is to implement and deploy an automated detector and localization model to locate underwater marine organisms using their low-frequency pulse sounds. This model is based on time difference of arrival (TDOA) and uses a two-stage approach, first, to identify the sound and, second, to localize it. In the first stage, an adaptive matched filter (MF) is designed and implemented to detect and determine the timing of the sound pulses recorded by the hydrophones. The adaptive MF measures the signal and noise levels to determine an adaptive threshold for the pulse detection. In the second stage, the detected sound pulses are fed to a TDOA localization algorithm to compute the locations of the sound source. Despite the uncertainties stemming from various factors that might cause errors in position estimates, it is shown that the errors in source locations are within the dimensions of the array. Further, our method was applied to the localization of Goliath grouper pulse-like calls from a six-hydrophone array. It was revealed that the intrinsic error of the model was about 2 m for an array spanned over 50 m. This method can be used to automatically process large amount of acoustic data and provide a precise description of small scale movements of marine organisms that produce low-frequency sound pulses. © 2023 Acoustical Society of America.
https://doi.org/10.1121/10.0017804

I. INTRODUCTION

More than 800 kinds of fish are capable of making noises for a variety of functions, according to research (Kaatz, 2002; Looby *et al.*, 2022; Rountree *et al.*, 2006; Ruppel *et al.*, 2022). Soniferous fishes include some of the most common and significant commercial fish species, such as codfishes (*Gadus morhua*), drum fishes (*Sciaenidae*), grunts (*Haemulon flavolineatum*), grouper (*Epinephelinae*), jacks (*Caranx hippos*), and catfishes (*Siluriformes*; Rountree *et al.*, 2006). Mussels (*Mytilus edulis*), sea urchins (*Echinoidea*), and other invertebrates that are vital to fisheries make sounds as well (Fish, 1964), such as white shrimp (*Penaeus setiferus*; Berk, 1998), spiny lobsters (*Palinuridae*; Fish, 1964; Moulton, 1957; Patek, 2002), American lobster (*Homarus americanus*; Fish, 1966; Henninger and Watson, 2005), and squid (*Teuthida*; Iversen *et al.*, 1963). Low-frequency sounds make up the majority of the sounds (Ladich, 2004), often at or below a frequency of 1000 Hz. Some pulses, on the other hand, can reach 8 kHz (Tavolga *et al.*, 1981; Zelick *et al.*, 1999) or might exhibit more complicated characteristics (Vasconcelos *et al.*, 2011). These emissions often consist of broadband short-duration signals as well. Fish use a variety of mechanisms to produce sounds, which vary depending on the

species and the situation, such as courtship, threats, or territorial defense (Kasumyan, 2008). Feeding activity, such as durophagy (shell crushing) can also be a contributor to the marine soundscape (Ajemian *et al.*, 2021).

Pulses associated with fish sounds can be categorized in terms of the number of pulses, pulse period, frequency, oscillogram shape, or a descriptive name or onomatopoeic word (like a growl, pulse train, or boom). As shown by Jublier *et al.* (2020), fish sounds recorded at a reef site in the southern Pacific Ocean consisted of various combinations of short low-frequency pulses between 30 and 800 Hz, including single pulses, which are called booms. Higher frequency clicks between 900 and 1200 Hz were also heard. These types of frequency clusters are present in the acoustic field of shallow-water coastal environments in tropical and temperate waters (Kennedy *et al.*, 2010; Radford *et al.*, 2010; Staaterman *et al.*, 2013). According to Coquereau *et al.* (2016), crustaceans are also known to create pulse-based sounds with frequencies ranging from 2.5 to 41 kHz, which are connected to a variety of behaviors, including feeding and snapping. Ajemian *et al.* (2021) revealed that shell fracture event by feeding organisms can be characterized as broadband pulses, spanning 400–22.1 kHz for preys such as hard clam and fighting conch among others. Even though the signals were wideband (WB), the mean frequency of highest energy (also known as the peak frequency) for all of the prey items was consistently centered between 2.9 and

a)Electronic mail: aaltaher2018@fau.edu
b)Also at: Harbor Branch Oceanographic Institute, Florida Atlantic University, Fort Pierce, FL 34946, USA.

4.3 kHz for the first fracture and 3.1 and 5.0 kHz when taking into account all of the fractures.

Low-frequency sound is also used by whales and seals for communication and environmental sensing (Tyack, 1998). Due to their spectral and temporal characteristics, the clicks made by sperm whales, beaked whales, and porpoises are distinctly different from those made by delphinids (Goold and Jones, 1995; Johnson *et al.*, 2006; Kamminga, 1996; McDonald *et al.*, 2009; Zimmer *et al.*, 2005). The bio sonar clicks of toothed whales observed to date, with the exception of beaked whales, can be broadly divided into ($<150\,\mu$s) broadband transients, produced by most delphinids (Au, 1993), or longer-duration narrowband high-frequency clicks, which some small toothed whale species generate (Madsen *et al.*, 2005). The third type are the low-frequency, multiple-pulsed clicks made by sperm whales (Møhl *et al.*, 2003).

The main common denominator between the sounds previously described, whether by toothed whales, fish, or crustaceans, in particular, in the narrowband type, is the characteristic waveform that is unique to each of the calls or elements of the calls (Fig. 1). Therefore, the detection of known structure in the signal can be used to identify the sounds of the different species. One of the best documented problems in communications (Wozenkraft and Jacobs, 1965), pattern recognition (Duda *et al.*, 1973), and image processing (Jain, 1989) is the ability to detect an object or pattern in a known deterministic signal in the additive Gaussian noise. Using matched filtering is the simplest and most effective technique (Wozenkraft and Jacobs, 1965). With a maximized signal-to-noise ratio (SNR) and minimized detection error probability, the matched filter (MF) is optimal when the noise is white (or the spectral density is known) and synchronized (i.e., the signal arrival time is also known). Precise temporal localization of animal borne sound pulses in acoustic records can, thus, be used to identify the animal location and, ultimately, its spatial distribution over time.

Precise pulse localization can be achieved by triangulation, beamforming (Ferguson, 1989; Van Veen and Buckley, 1988), wave fingerprinting (del Hougne *et al.*, 2021; del Hougne, 2020; del Hougne *et al.*, 2018; Ing *et al.*, 2005), and time-reversal mirror (Zeldovich *et al.*, 1985). Based on the time difference of arrival (TDOA), the triangulation concept can be used to estimate the range and bearing of the sound source (Carter, 1979; Ferguson and Lo, 2002; Wu and Zhu, 2010). The TDOA method is typically used in long baseline (LBL) systems to locate equipment underwater (Jakuba *et al.*, 2008). In TDOA-based localization, the difference in the measured time of arrivals of signals, received from a pair of reference nodes, is translated to the difference in range estimates with those reference nodes and gives rise to a hyperbola for the unknown position of the node (target node). A unique estimation of the target node position can be obtained by intersecting three such hyperbolas. However, this technique requires that reference nodes transmit at near concurrent time if the target node is
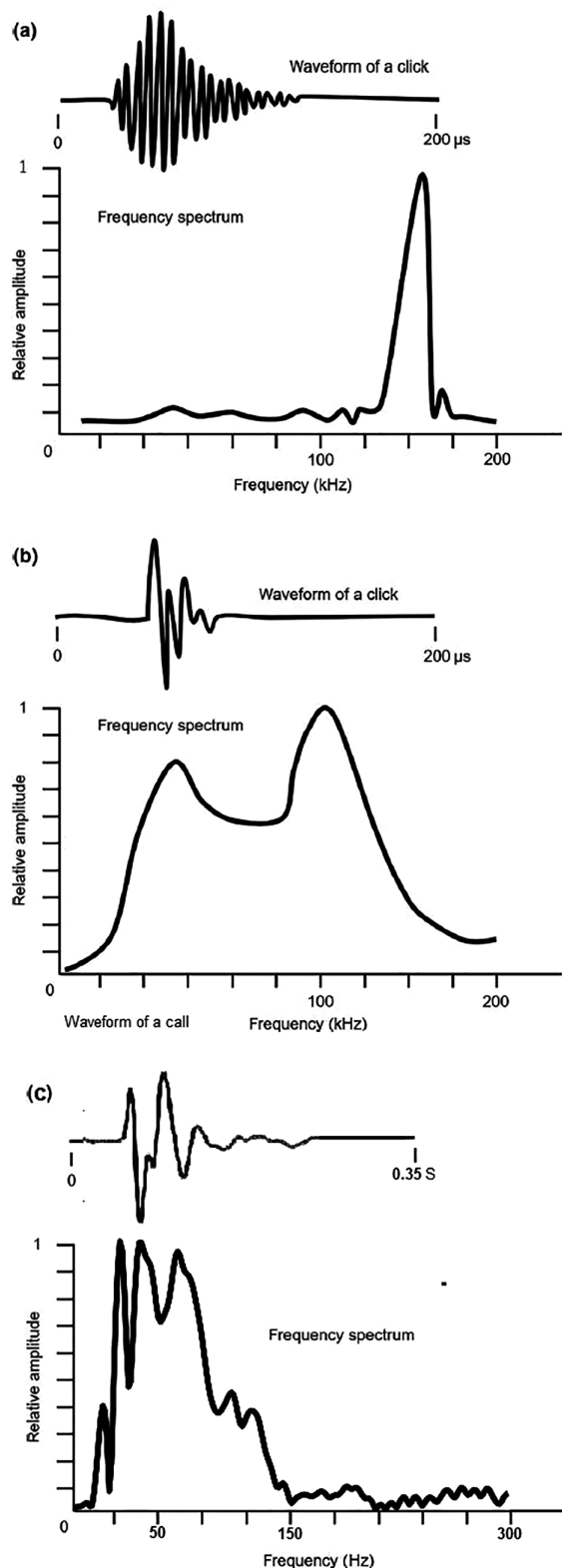
FIG. 1. Representative waveforms and frequency spectra of echolocation clicks of odontocetes and Goliath grouper (GG). (a) A narrowband high-frequency (NBHF) species *Phocoena phocoena* is redrawn from Au (1993), and (b) a WB species *Stenella frontalis* is redrawn from Au and Herzing (2003). NBHF clicks are longer in duration ($>120\,\mu$s) and have a sharper frequency peak at $>100\,$kHz; WB clicks are shorter (40–70 μs) and have a moderate frequency peak at 30–100 kHz. (c) A narrowband GG call. The pulse duration can be greater than 100 ms at a peak frequency of 60 Hz. [(a) and (b) are redrawn from Kuroda *et al.*, 2020.]

J. Acoust. Soc. Am. **153** (4), April 2023

Altaher *et al.*   2191

moving. A few studies on wild marine mammals have been able to overcome the problem of sound source detection by using passive acoustic localization (Janik, 2000; Wiggins *et al.*, 2013). These studies used TDOA at different transducers of a microphone array to determine the source position. Its main advantages are that it is completely noninvasive and can be used to monitor vocal behavior of several individuals at once. However, the accuracy of passive localization relies heavily on the acoustic topography of the study site (Spiesberger and Fristrup, 1990) and data analysis can be very time-consuming. In this study, we apply the TDOA method to the localization of fish calls recorded by a static hydrophone array distributed around the fish habitat. We show that this method lends itself to an automated identification and localization algorithm when coupled with a MF because it mitigates the multipath effect on the call's signal.

For the purpose of this study, we selected the low-frequency Goliath grouper (GG; *Epinephelus itajara*, Lichtenstein, 1822) calls. One of the largest grouper species, the Atlantic GG can grow to a length of 2.5 m and weigh more than 400 kg (Bullock *et al.*, 1992). The species is found in the Gulf of Mexico and spreads from North Carolina to Brazil (Bertoncini *et al.*, 2018). Low-frequency pulses of the GG consist of a narrowband low-frequency pulse of relatively long duration (>110 ms) with a peak at 60 Hz (Mann *et al.*, 2009). The GG "booms" show a "polycyclic" waveform, which rapidly increases in amplitude for up to one or two wave cycles and then decays exponentially [Kuroda *et al.*, 2020; Fig. 1(c)]. Despite studies shedding light on site fidelity and coarse horizontal and vertical mobility based on acoustic telemetry research (Collins, 2014; Malinowski *et al.*, 2019; Mann *et al.*, 2009), no studies have described this species' fine scale behavior as of yet. Localizing grouper calls around their habitat can provide the opportunity to learn about fine scale GG activity patterns over a range of temporal scales, ambient noise, and environmental conditions. The localization method presented in this study is, therefore, applicable to similar sounds pulses emitted also by whale, delphinids, and crustaceans.

The paper is organized as follows. Section II details the methodology used in this study, including data collection, call detection and timing, and source localization. An adaptive MF is used twice, first, to detect the GG calls and, second, to extract their time of arrival at each hydrophone of the array. Then the TDOAs are used in a localization algorithm to compute the locations of the grouper calls. Section III presents simulations of the sensitivity of the algorithm to TDOA and placement errors of the hydrophones. The detection and localization model is then applied to the horizontal array data to localize the grouper calls. The accuracy of the model is estimated with the known location of a pulse-like sound source. The results of the GG call localization are also compared to a manual estimation of the TDOA, substantiating the accuracy of the MF at estimating the call timing. Conclusions are given in Sec. IV.

II. METHODOLOGY

In this section, we provide the experimental setup along with a description of the acoustic array used to study the call-based distribution of GG near their habitat. It is followed by a detailed description of the novel adaptive MF and a mathematical presentation of the localization algorithm.

A. Experimental setup

The GG is a coastal species that is found mostly in high relief artificial and natural reef at varying depths between 0 and 30 m deep (Malinowski *et al.*, 2019). It is a gregarious species, and some sites can host a large number of fish (>10 individuals) year-round. To assess fish presence by measuring fish acoustic activity and the fish distribution relative to their habitat, we deployed a battery-powered six-element acoustic array at one artificial reef off of the west coast of central Florida (Fig. 2), which recorded continuously for 3 days in June 2019. The site selected for this study was MD-1, which consists of sunken steel barge on a sandy bottom in 24 m of water. The highest point of the artificial reef is about 3 m above the bottom. The six-element acoustic array was set up such that three hydrophones were on the structure and three hydrophones were on the ocean floor around the wreck. Measurements between the various hydrophones were made by divers using a 100 m transect tape and recorded onto an underwater slate to the nearest centimeter. These measurements were used to digitize the array using the recorded distances between hydrophones in concert with visual landmarks of the wreck from a georeferenced image in ArcMap 10.3 (ESRI, Inc., Redlands, CA).

The acoustic array was composed of a Zoom H6 Handy off-the-shelf portable six track acoustic recorder (Hauppauge, NY) with six High Tech Instruments (HTI,

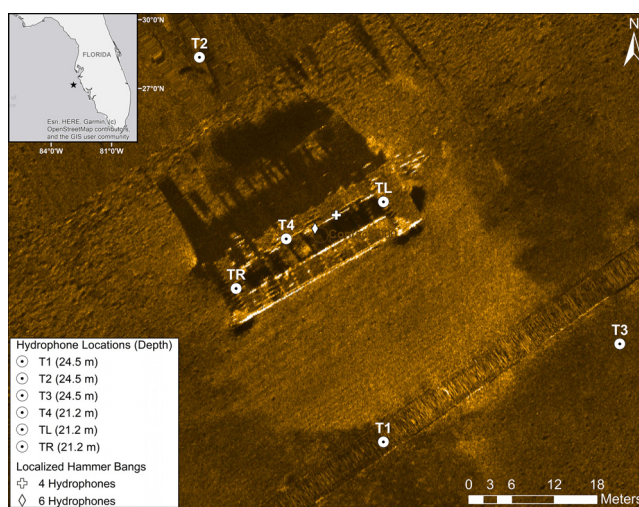FIG. 2. (Color online) Side scan sonar image of the experimental site MD1, off of the west coast of Florida. The relative positions of the six hydrophones used in the simulations and experimental studies are shown by the white labels. Hammer bangs were recorded and produced near T4. The localized hammer bang positions with the four- and six-hydrophone models are shown by the cross (+) and diamond (⌑), respectively.

Long Beach, MS) hydrophones. Figure 2 shows the layout of the hydrophones. In this experiment, hydrophones TR, T4, and TL were located on the wreck and T1, T2, and T3 were located on the ocean floor. The Zoom H6 was programmed to record continuously at 44.1 kHz and powered with four, six-pack 4.5 V D-cell alkaline battery connected in parallel. Data were recorded to a 512 Gb secure digital flash memory card. The sensitivity of the hydrophones in the system was −186 dB (re: 1 μPa). The recording system was placed in a polyvinyl chloride (PVC) underwater housing and weighted with 7 kg to achieve negative buoyancy. Cabled hydrophones were placed at various distances to calculate time of arrival differences between recording tracks (each hydrophone was on a different recording track) to estimate the position of sound sources. Due to the meandering layout of the cables connecting the hydrophones, the precise positions of these hydrophones were unknown. The location errors were estimated to be on the order of 1–2 m. However, hammer bangs at known locations within the array were recorded to validate the localization model, and the manual call timing analysis was used as a reference method for the automated model. Sound velocity profiles (SVPs) at the location of the array were recorded over 2 days during the deployment (Fig. 3). The sounds speed decreases toward the bottom. The largest velocity change is found between 10 and 15 m, after which the sound speed varies around 1545 m s^{-1}. This variation is caused by the presence of salty water from the Loop Current (Chérubin and Burgman, 2022), which creates a pycnocline between 10 and 15 m. It is not a typical profile because Loop Current intrusions are transient. Away from the Loop Current influence, West Florida shelf waters typically exhibit a seasonal variability, which consists of well mixed water in the winter with a progressive summer stratification toward the surface with some diurnal variation (Weisberg and He, 2003).
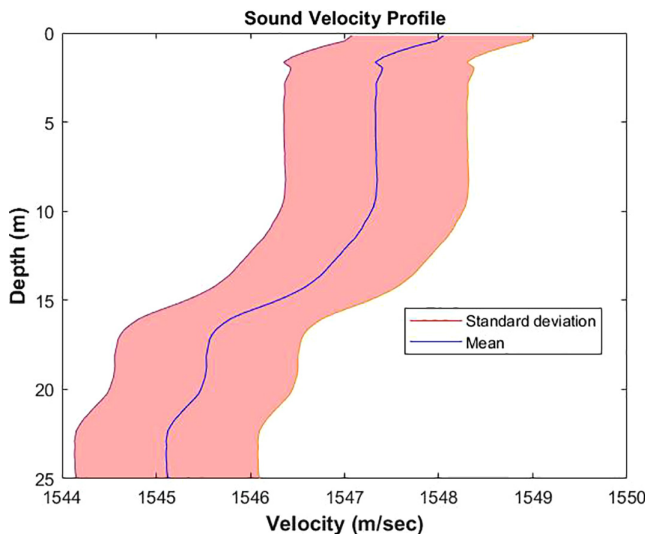

FIG. 3. (Color online) Water column SVP mean and standard deviation measured at the experimental site MD1 during the three-day experiment in June 2019.

B. Adaptive MF for call detection and timing

The adaptive MF was designed to detect grouper calls and record their timing for the localization step. A two-pass procedure is employed for these tasks. In the first pass, GG calls are detected, and in the second pass, the timing of the calls is determined and provided to the TDOA localization algorithm. Both tasks are completed with an adaptive MF. The functional diagram of the adaptive MF for the call detection is displayed in Fig. 4. The filter uses two templates: one template is the waveform of a typical GG call, and the other template is a waveform of ocean ambient noise, both are from the acoustic records used in the study. The GG call template is selected through trial and error such that it yields the highest call detection for the selected dataset. The ocean ambient noise template is used to adaptively scale the threshold value of the MF output. The gain factor, Kd, for the threshold value is experimentally chosen to maximize true positive detections and is unique to the dataset. In this study, its value was set to 0.9.

The detection step is as follows. The signal is first broken into 20 s segments. This time length was selected because it gave better results for the threshold value. After low pass filtering of frequencies above 150 Hz, the input signal is convolved with the grouper call template (top path in Fig. 4) and ambient noise template (bottom path in Fig. 4). The mean of the second convolution is calculated and then multiplied by the gain factor Kd to determine the threshold value, with which the convolution result is converted to a binary decision on whether the input signal is a grouper call or not. An example of the filter output with threshold level is given in Fig. 5.

To estimate the timing of the call through each hydrophone, the waveform of the detected GG call is isolated from the input signal using a dynamic window that fits the detected call [Fig. 6(b)] and considered as the updated template for the MF. This approach mitigates the propagation effects, including multipath that could modify the signal from the fish. The dynamic window size is defined by the start and end of the call in its energy form. The 20 s segment energy is, thus, averaged across all of the frequencies. For each call detected in the 20 s segment, we used a threshold value set to zero such that the call window is defined by positive values of the energy. Our experiment has shown that choosing zero as the threshold value produced proper window sizes for the second pass. The MF is, thus, applied a second time to the detected call over the selected energy window, using the call itself as a template to identify the time of the call. Within the energy window, the template is correlated with the signal while it is moved along the time axis, and the time at which the highest correlation coefficient is obtained is marked as the relative time of arrival. This sequence is repeated for each call in the 20 s segment if any.

C. Mathematical model for sound pulse localization

After the timing of a GG call is determined, the corresponding TDOAs can be computed and, then, the location of

J. Acoust. Soc. Am. **153** (4), April 2023
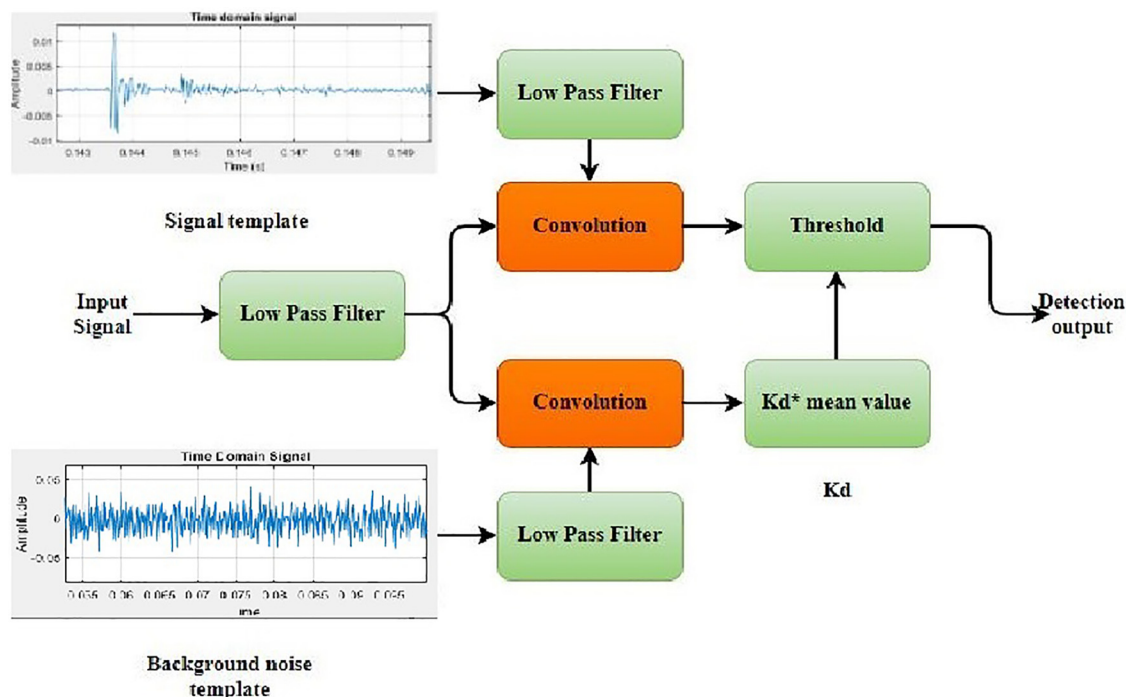
Altaher *et al.* 2193

FIG. 4. (Color online) Functional diagram of the adaptive MF. The top convolution determines the matching score between the input signal and the desired signal template. The bottom convolution determines the threshold value, which is the mean of the result of the second convolution multiplied by a gain factor (Kd), with which a decision on whether the input is a desired call or not is made.

the grouper call can be estimated. Ground-truth measurements or, more typically, simulations can be used to assess TDOA localization sensitivity to TDOA estimate errors. Other factors contribute to the inherent error in the TDOA method. They consist of uncertainty in receiver placements, environmental variables (sound speed, bottom type, etc.), and propagation effects (Spiesberger and Fristrup, 1990).

TDOA inherent errors are also related to the signal's acoustic characteristics (Carter, 1987), the number of receivers counted in the localization (Spiesberger and Fristrup, 1990), the SNR of the signal received (Cespedes et al., 1997), and the effect of broadband noise at low SNR (Azaria and Hertz, 1984), as well as the presence of other signals (Wiggins et al., 2013).
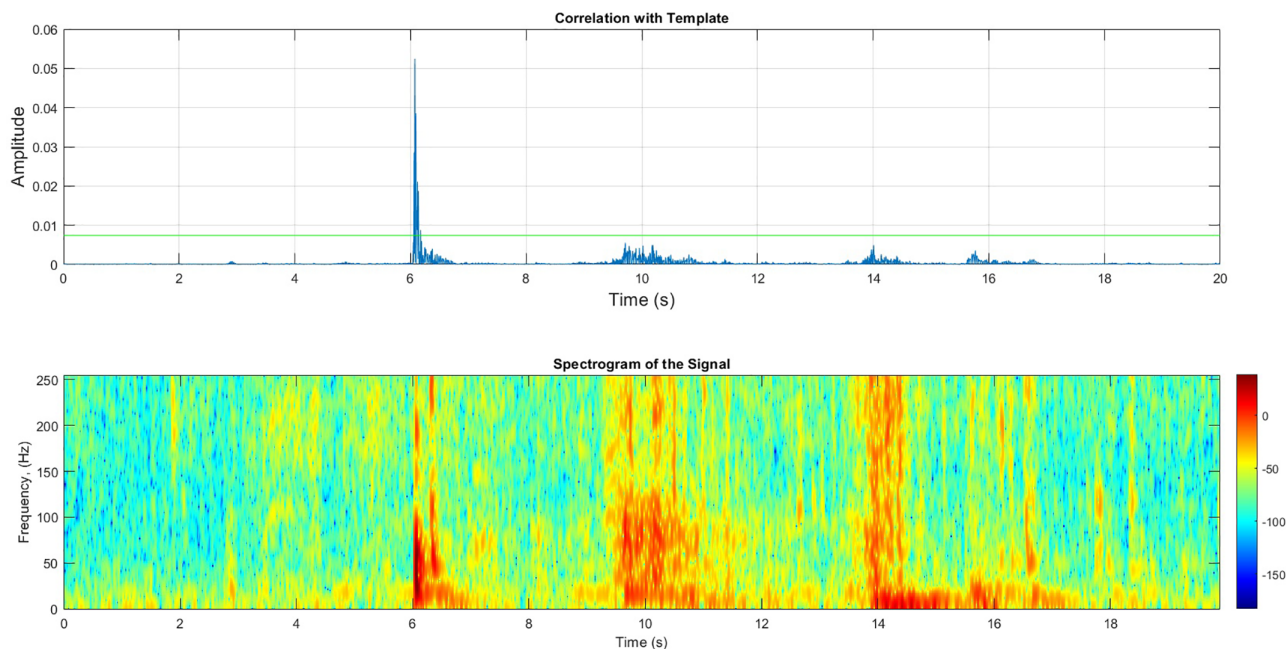

FIG. 5. (Color online) An example of the output of the adaptive MF for the first pass (top). The green line shows the threshold value, and the blue line shows the GG call convolution. The bottom diagram shows the spectrogram of the audio segment (dB) used in this example.

2194   J. Acoust. Soc. Am. **153** (4), April 2023
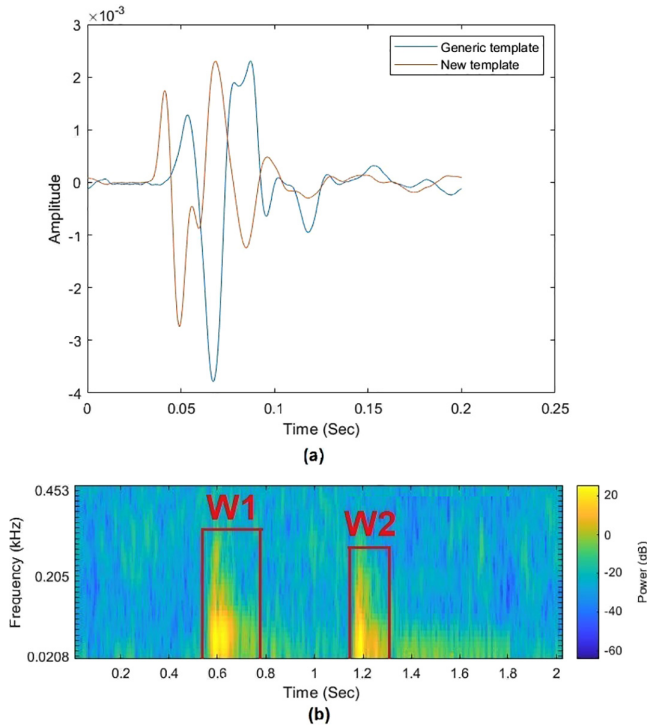
Altaher et al.

FIG. 6. (Color online) Examples of waveform of the MF templates and call detection windows. (a) Waveform of the generic template used by the MF to detect a GG call, and the waveform of an updated GG call template used to determine the time of arrival of the GG call. (b) GG calls spectrogram with call windows are outlined in red. W1 and W2 stand for window 1 and window 2, respectively. The width of detection window varies to accommodate duration variation of GG calls.

Three-dimensional localization can be achieved with three receivers when the distances between the source and receivers are known and with three or more noncollinear receivers using TDOA measurements (Kunin, 2010). The basic geometry and parameters with four receivers arranged in a space is shown in Fig. 7.
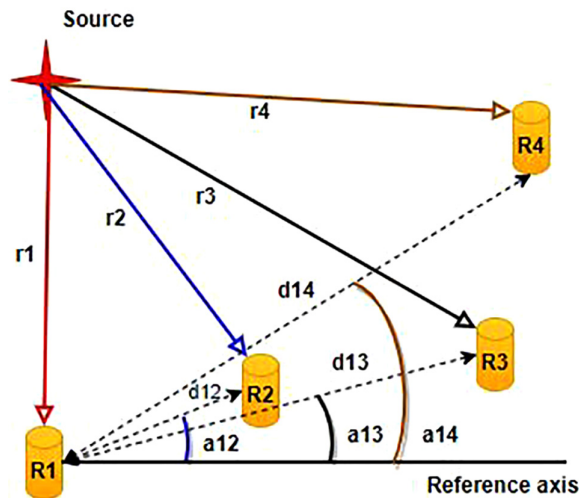

FIG. 7. (Color online) Three-dimensional localization geometry. Reproduced from Kunin (2010).

In this model, d12, d13, and d14 are the distances between the receiver R1 and receivers R2, R3, and R4, respectively, and a12, a13, and a14 are the angles between the reference axis and R1, R2, and R3, respectively. The distances between the receivers and the source are denoted by r1, r2, r3, and r4. x, y, and z are the coordinates of the source under investigation. The equations below summarize the mathematical representation of the system configuration:

$$r1 = x^2 + y^2 + z^2, \tag{1}$$

$$r2 = x^2 - 2 * d12 * x + y^2 + (d12)^2 + z^2, \tag{2}$$

$$r3 = (d13 * \cos(a13) - x)^2 + (d13 * \sin(a13) - y)^2 + z^2, \tag{3}$$

$$r4 = (d14 * \cos(a14) - x)^2 + (d14 * \sin(a14) - y)^2 + z^2. \tag{4}$$

Considering Eqs. (1)–(4), the TDOA relations can be expressed as

$$a = r3 - r1 = TDOA13, \tag{5}$$

$$b = r3 - r2 = TDOA23, \tag{6}$$

$$c = r4 - r2 = TDOA24. \tag{7}$$

Substituting Eqs. (1)–(4) into Eqs. (5)–(7) results in a set of linear equations that can be solved for x, y, and z, which are the coordinates of the source. In the following, the four-hydrophone model based on the first three TDOAs presented here will be compared to a six-hydrophone model based of the first five TDOAs presented here. It is expected that adding more TDOAs or increasing the number of hydrophones increases the precision of the localization model significantly.

III. RESULTS

A. Errors simulation and analysis

In this section, we present the results of the simulations using four and six hydrophones, respectively, that were conducted to test the sensitivity of the localization method to (1) the effects of the TDOA measurements, and (2) the effects of the localization model parameters, which are related to the uncertainties in the placements of the hydrophones. The accuracy of TDOAs is directly linked to GG call timing by the MF described in Sec. II B, and the accuracy of the model parameters is related to the location of the hydrophones in the system (Sec. II A).

For the first simulation, the TDOA between each pair of receivers was determined for one thousand sources spread randomly within a 500 m radius of the array's center. For all simulations, the delays for each assumed source site were computed using a sound speed of 1545.4 m s^{-1} under the conditions of temperature of 29.2 °C, salinity of 36.2 psu, and a normative depth of 20 m, as measured at the
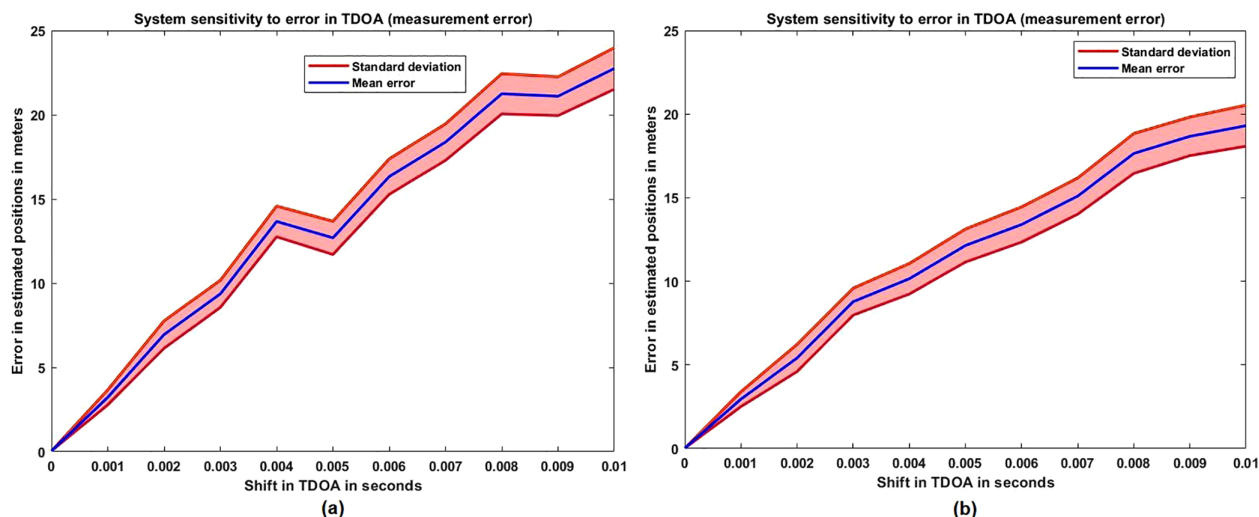
FIG. 8. (Color online) Source localization error as a function of TDOA measurement errors (blue line). The shaded area shows the standard deviation of the localization error. The (a) four-hydrophone set model and (b) six-hydrophone set model are shown.

experimental site. To estimate the three-dimensional locations, these estimated TDOAs were fed into the localization model, which was represented by a system of linear equations. It was solved by the Lower-Upper (LU) factorization method. For each simulated position, 10 000 trials were performed, and the average of Euclidean distances was used as the mean error corresponding to the TDOA error at a given level (e.g., 0.001, 0.002 s, and so on). The results are shown in Fig. 8.

The graph shows that the error in position estimation depends almost linearly on the TDOA error. It also emphasizes the importance of the second pass of the MF with the updated template over the records, which resulted in a reduction in TDOA measurements errors that were in the microsecond range (not shown). Indeed, the timing of the calls could be directly obtained from the detection stage MF. However, the call timing showed significant differences

with the ones obtained with the second call specific MF. Errors of the localization can, thus, be significant as shown by the simulation and confirmed by the localization verification experiment described in Sec. III B. The errors produced by the six-hydrophone model were, in general, less than those by the four-hydrophone model, as shown by Fig. 8.

In the second simulation, the TDOA between each pair of receivers was determined for 1000 virtual source locations, but errors were incrementally added to the location of the hydrophones (e.g., 0.2m, 0.4 m, and so on). The error range of the hydrophone position was based on the average error corresponding to each increment of the position errors. The results of the second simulation are depicted in Fig. 9. Again, the position error is almost proportional to the shift in hydrophone positions. It also shows that the source location errors are within the dimensions of the array (<20 m) within a tenfold change in TDOA or relative position error.
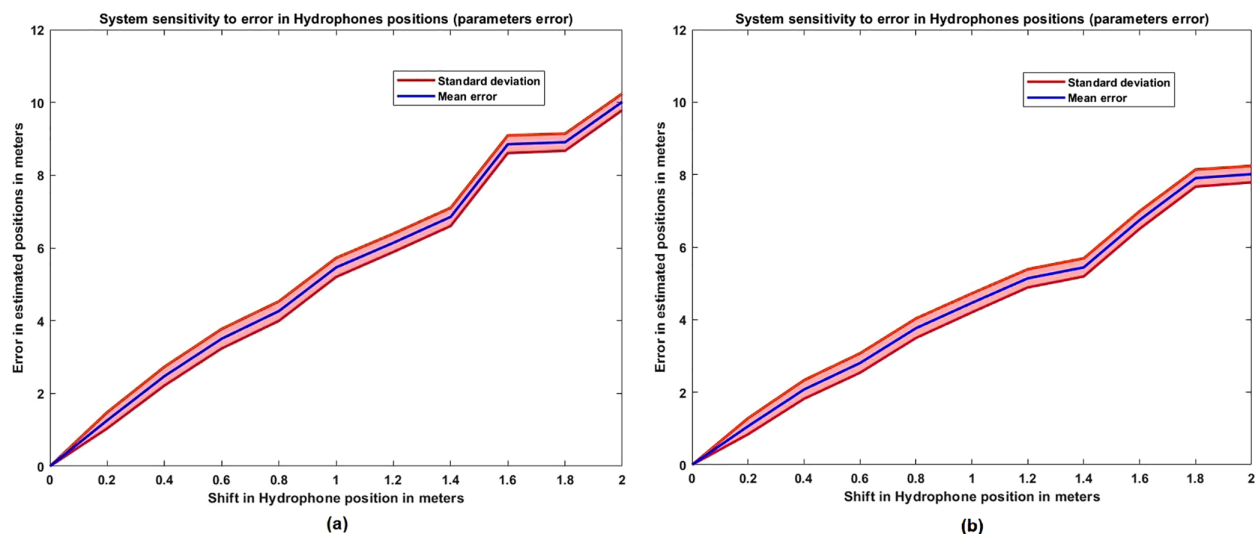

FIG. 9. (Color online) Source localization error as a function of hydrophone position errors (blue line). The shaded area shows the standard deviation of the localization error. The (a) four-hydrophone model and (b) six-hydrophone model are shown.

Again, the results show that the errors produced by the six-hydrophone model were, in general, less than those produced by the four-hydrophone model, as shown by Fig. 9.

B. Inherent localization error of the cabled array system

To validate the automated localization model for pulse sounds like GG calls, the four- and six-hydrophone models were tested on hammer bangs recorded by the array, whose locations were known. The bangs were manually recognized in the recordings, and the TDOAs between them were also calculated using the two-pass MF. The positions were calculated by considering a sound speed of $1545.4 \, \text{ms}^{-1}$ for a temperature of $29.2 \, ^\circ\text{C}$, salinity of 36.2 psu, and normative depth of 20.0 m, measured at the time of the hammer bangs and used for the rest of the recording period. Figure 2 illustrates the position for one of the detected hammer bangs. The errors of the bang positions are 2.45 and 4.37 m for the six- and four-hydrophone models, respectively, with regard to where the bang was originally generated, near T4. Both locations are on the wreck. This result provides an estimate of the true localization error using real data, which inherently have uncertainties not simulated or associated with recorder synchronization, receiver positions, and acoustic propagation. The hammer bang was also used to estimate the accuracy of an algorithm based on just one MF, the algorithm associated with the detection of the call, from which the timing was obtained. It located the same hammer bang off of the wreck, about 20 m southeast

of TL. The three-hydrophone model also located the hammer bang off of the wreck about 11.4 m southeast of TL, which speaks to the advantage of increasing the number of hydrophones of the array to increase the precision but also to increase redundancy with more hydrophones if the sound source is absent in the recordings of one or more hydrophones.

C. Grouper call localization

To validate the automated localization model of grouper calls, we computed the locations of a set of 50 GG calls by manually calculating the TDOAs with 3, 4, and 6 hydrophones, respectively. The TDOAs for each call were calculated with reference to the first received hydrophone record from which the time of arrival at the other hydrophones is subtracted to obtain the TDOAs used in localization algorithm. The manual method relied on identifying the start and end of the call visually and use the time in the middle as the time of arrival. We defined this as the center of the call. The difference between the manually and MF calculated calls are shown for a few examples in Fig. 10. Despite the difference in methods, the results show agreement between the methods regarding the timing of the calls. If the relative call timing differences between the two approaches, manual and automated, were identical for each detected call, then the manual and automated methods should give the same localization results. As shown below, human-machine timing differences can lead to significant deviations in the source localization (Table I). Table I provides the worst and best
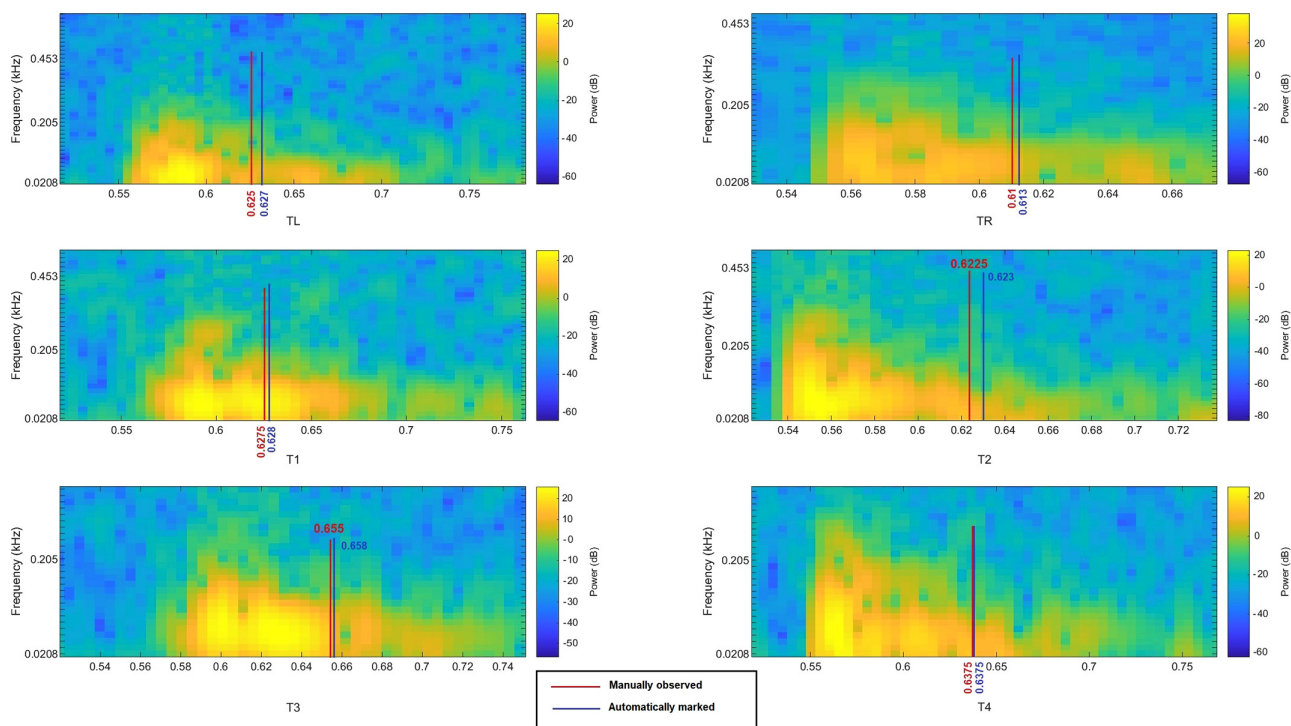
FIG. 10. (Color online) Call timing determination. Manually (red lines) and MF (black lines) located call centers for six different calls are depicted. In the manual method, the timing of the call arrival is determined by the center of the start and end intervals of the call. In the automatic method, that is determined by the timing at which the MF produces the highest auto-correlation value.

J. Acoust. Soc. Am. **153** (4), April 2023

Altaher et al.   2197

TABLE I. Comparison between manual and MF call detection with a three-, four-, and six-hydrophone model. Δ denotes the differences between the results of the automatic and manual methods. Columns 2, 4, and 6 show the differences of the TDOA means, columns 3, 5, and 7 show the distances between manually and machine estimated source locations, and columns 6, 7, and 8 show the percentage of the former over the manually estimated distance between the source locations and the center of the array. The last column provides the latter. NA indicates failure to detect a fifth call.

Call number	Three-hydrophone model Δ (s)	Three-hydrophone model Δ (m)	Four-hydrophone model Δ (s)	Four-hydrophone model Δ (m)	Six-hydrophone model Δ (s)	Six-hydrophone model Δ (m)	Three-hydrophone model Δ (%)	Four-hydrophone model Δ (%)	Six-hydrophone model Δ (%)	Call position (m)
1	0.00033	3.5	0.000875	2.8	0.00145	2.1	8.7	7	5.22	40.23
2	0.000332	3.9	0.000895	3	0.0015	2.23	8.6	6.6	4.91	45.35
3	0.0015	7.67	0.001605	7.45	0.0172	5.18	11.8	11.46	7.96	65
4	0.00143	4.7	0.001582	4.3	0.001755	3.41	5.59	5.05	4.05	84.08
5	0.002	4.67	0.00242	4.19	0.00728	3.727	4.57	4.1	3.65	102.188
6	0.0047	10.93	0.005	9.76	0.0119	8.62	15.6	13.94	12.3	70.06
7	0.001	6.01	0.00187	5.74	0.00383	5.1	4.62	4.41	3.92	130.09
8	0.007	18.52	0.0136	35.71	NA	NA	12.88	24.83	NA	143.82
9	0.00363	6.16	0.00685	5.94	NA	NA	10.26	9.9	NA	60.04

comparison cases between the manual and MF call localization methods.

Figure 11 illustrates the TDOA measurement differences for each of the calls in Table I. Those results show, basically, what the simulation of the effect of TDOA differences previously revealed. The mismatch between the manually and automatically computed times of arrival at the hydrophone is responsible for the difference in location of the sound source. The manual and MF methods can be relatively close as shown by Figs. 10 and 11. Slight differences in TDOAs consist of various types of mismatch scenarios such as (1) the time sequence of the times of arrival is the same between manual and automatic detection, however,

the individual TDOAs might slightly differ [Figs. 11(a) and 11(b)]. (2) The time sequence of the TDOAs differs between both methods in addition to the differences between individual TDOAs. In the latter case, the errors are compounded and the source location difference can be significantly greater than in the previous case as shown by calls 3, 4, and 6 [respectively, Figs. 11(c), 11(d), and 11(f)]. (3) The third possible case is associated with the selection of a different set of hydrophones for call localization, as shown by Figs. 11(c), 11(d), 11(f), 11(h), and 11(i) [or calls 3, 4, 6, 8, and 9 (Table I)]. For example, in Fig. 11(c), there is a set of five manually detected calls to choose from that is different from the set of four MF detected calls. In the case of four
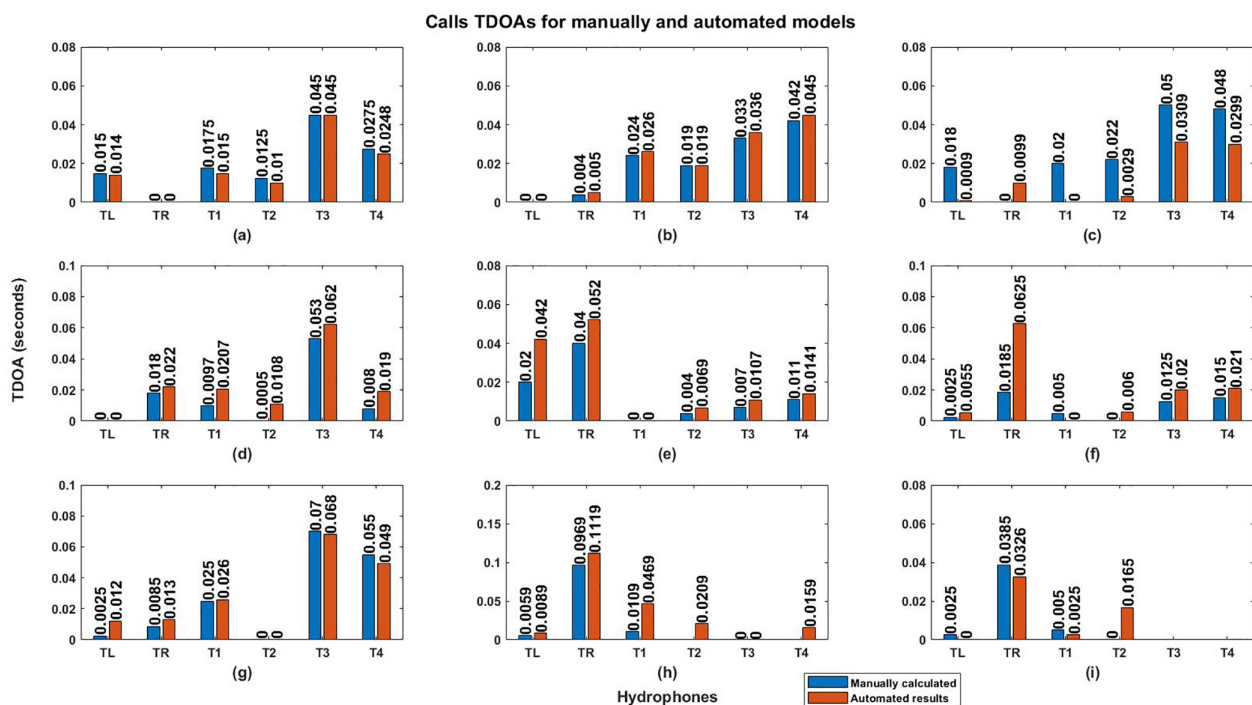

FIG. 11. (Color online) TDOAs calculated manually at each hydrophone of the array and automatically by the MF. The labels on the x axis indicate the hydrophones of the array. The first two, first three, and first five TDOAs are used by each model. Calls (a)–(i) represent calls 1–9 in Table I, respectively.

2198   J. Acoust. Soc. Am. **153** (4), April 2023
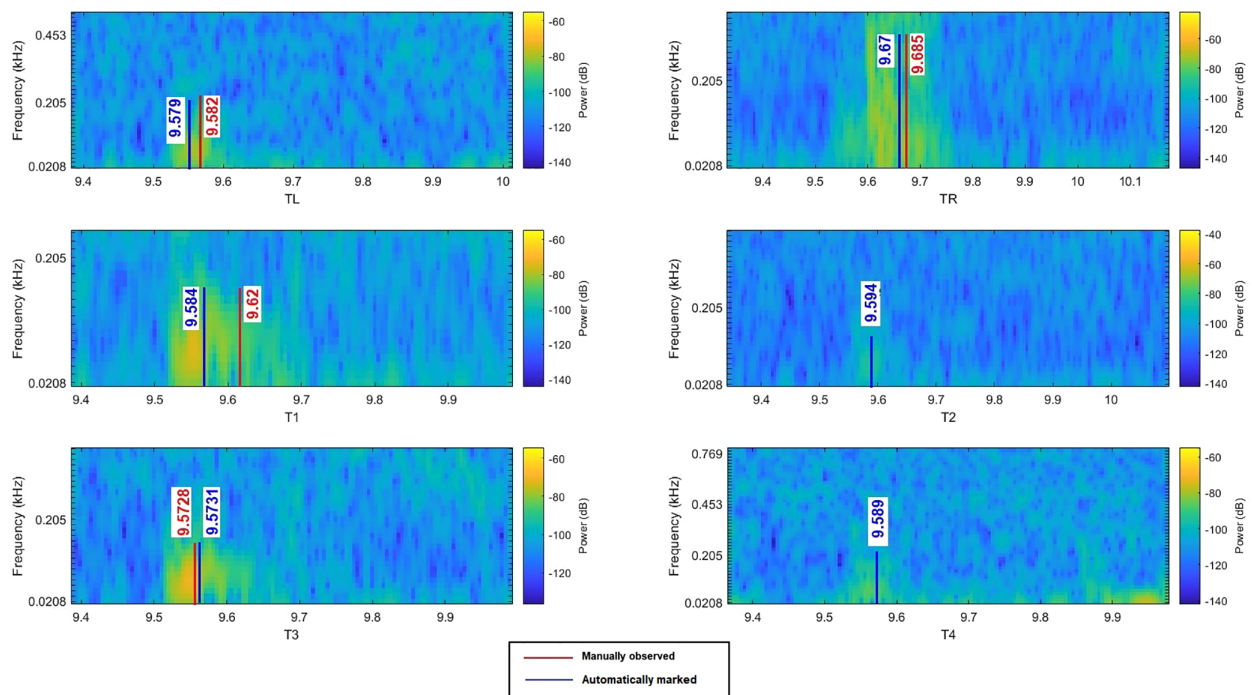
Altaher et al.

FIG. 12. (Color online) Spectrograms of call 8 (Table I) and manually (red lines) and automatically (blue lines) marked times of arrival recorded at each hydrophone of the array. The label under each graph indicates the name of the hydrophone.

hydrophones used for the localization, this type of difference can lead to the greatest difference in localization as shown by call 8 (35.71 m; Table I).

Figure 12 illustrates why the distance estimated by the manual method can be so different from that of the automatic method. The SNR is relatively low at some of the hydrophones, which makes it difficult to visually mark the center of the call. For example, the manually marked time of received call at T1 is questionable, although it seems to be at the center of the call whose duration seems to span from 9.52 to 9.7 s. At hydrophones T2 and T4, the call is not identifiable as a GG call and not marked. It is, however, identified by the MF. This example shows that the MF-based call center identification is more robust, even when the SNR is low.

D. Application to GG habitat kernel distribution

Atlantic GG are likely to be present and occur in greater abundance at artificial reefs. Collins *et al.* (2015) observed that abundance was positively related to vertical relief and structural volume, and the largest numbers of individuals were observed at high volume artificial reefs (e.g., shipwrecks). Likely, this was due to greater refuge availability provided by artificial reefs within the study region, where structurally comparable natural habitats are rare. Individuals are sedentary and display high site fidelity through most of the year, except during reproductive periods (August–October) when they may travel hundreds of kilometers to reach spawning aggregations (Collins, 2014; Koenig *et al.*, 2011; Koenig and Coleman, 2013; Sadovy and Eklund, 1999). Site specific observations have shown that the fish tend to aggregate in a specific area of

their habitat where they will be observed most of the time. Sound production analysis of GG in long-term acoustic recording on two sites, in the Gulf of Mexico off of the southwest coast of Florida, documented that sounds were most frequently produced between 01:00 and 03:00 h (Mann *et al.*, 2009). Here, we used the automated call localization approach to map the distribution of GG calls at the artificial reef where the array was deployed at two specific times of the day, as displayed in Fig. 13. The distribution was created by implementing a kernel density function in ArcGIS (Redlands, CA) that calculates the density of calls per unit area. Midday distribution shows a cluster of fish located near the center and to the north and east of the wreck [Fig. 13(a)]. During the night, the cluster of fish calls is more centered near the wreck and to the southwest of it [Fig. 13(b)]. Although less calls were detected during the night window, this type of analysis can provide further insight into the kernel distribution of the fish near its habitat, which remains unknown to this day. Such information is useful to understand fish response and behavioral change to environmental changes and anthropogenic disturbance, such as ocean noise and fishing activity, but also environmental changes associated, for instance, with warming waters due to climate change (Pinsky *et al.*, 2020) or red tides that now frequently occur on the west coast of Florida (Weisberg and Liu, 2022).

IV. CONCLUDING REMARKS

Underwater pulse-like sounds can be produced by a variety of marine organisms such as marine mammals, fishes, and invertebrates. We showed that these animal sound pulses exhibit similar characteristics. Their polycyclic

J. Acoust. Soc. Am. **153** (4), April 2023
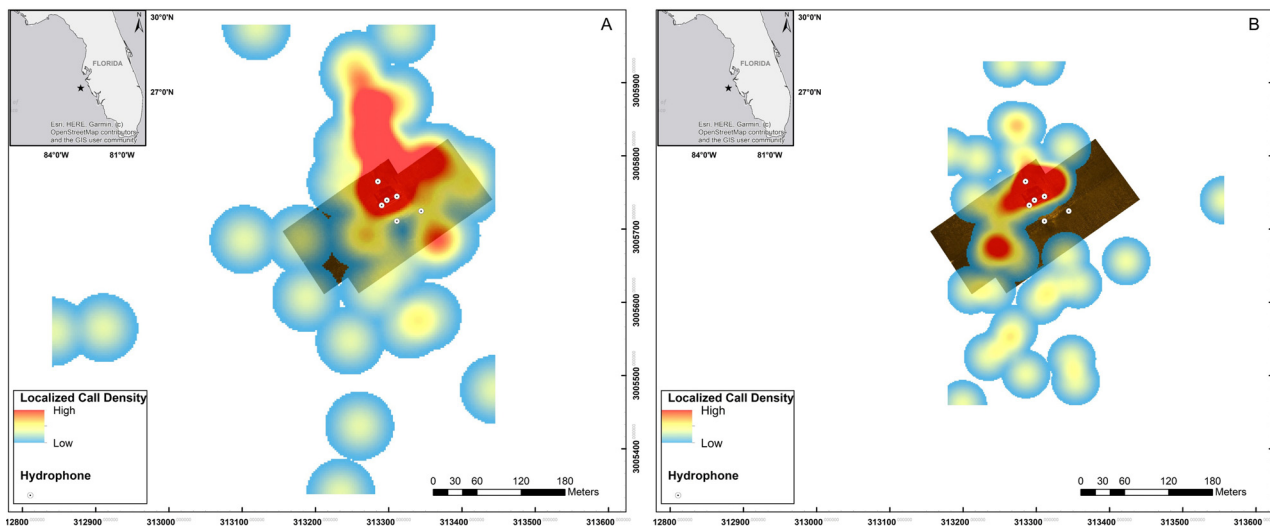
Altaher *et al.* 2199

FIG. 13. (Color online) The distribution of GG calls at two different times on a particular day, calculated by the automatic localization model. (a) The distribution between 10:00 and 12:00 h, and (b) between 01:00 and 03:00 h is illustrated.

or oligocyclic unique nature predisposes them to be uniquely identified by a method such as matched filtering, which uses a generic template of the pulse to be identified. In this study, we chose to use the pulse-like sound of the GG, a once common reef inhabitant of the subtropical and subtropical Atlantic coastal seas. It produces a single low-frequency polycyclic pulse that can be uniquely identified with a matched filtering technique.

In this paper, we presented a method for localizing single pulse-like underwater sounds using three, four, or five TDOAs from a six-hydrophone array. The latter almost guarantees that the sound will be captured by at least three receivers. To localize the calls, we implemented a two-step automated algorithm. First, the pulse-like sound is detected by using a generic adaptive matched-filter and, second, the TDOAs are also calculated with an adaptive, this time call-based MF. One could ask if using the MF detection alone would provide the same accuracy as the two-MF (detection and call timing) presented herein? Although the call timing can be obtained from the detected call, the cross-correlation peak between the generic template and call can significantly differ from the cross-correlation peak using the detected call as a template. Experimental results exhibited double the error of the hammer bang location obtained with the two-MF localization method.

The GG sounds used in this study were recorded at an artificial reef in the Gulf of Mexico, where the fine scale distribution of fish around their habitat was studied. This analysis was based on the localization of the fish calls, which was obtained with the model presented herein. The sensitivity of the localization algorithm was, thus, evaluated and two simulation studies were conducted. In the first simulation, the sensitivity of the proposed model to errors relative to the estimation of TDOAs by the MF was investigated. In the second simulation, the sensitivity of the model relative to the hydrophone position errors was evaluated. It revealed that the errors in GG call localization were proportional to the TDOAs and hydrophone position errors and within the array dimension for a tenfold error on TDOA and hydrophone relative position errors. We further evaluated the two-stage MF model with the *in situ* recordings of GG calls against a manual TDOA estimation. It showed that the MF approach is more robust to low SNR call identification and timing. The model accuracy was evaluated with the localization of hammer bangs near the center of the array. It shows an accuracy of $\sim 3m$, which supports the use of such an approach, in particular, the two-stage MF to localize biotic underwater sources using TDOAs from a distributed array of receivers. This automated approach enables the efficient processing of large acoustic datasets to continuously map the evolution of the sound source spatial distribution with relatively high precision. This method can be applied to track a group of marine organisms and their related activities, such as feeding for marine mammals or invertebrates, or in response to predators or mating partners, or any other disturbances within their habitat.

ACKNOWLEDGMENTS

Ajemian, M. J., Lamboy, C., Ibrahim, A., DeGroot, B. C., Bassos-Hull, K., Mann, D. A., and Chérubin, L. (**2021**). "Capturing shell-crushing by large mobile predators using passive acoustics technology," J. Exp. Mar. Biol. Ecol. **535**, 151497.

Au, W. W. L. (**1993**). *The Sonar of Dolphins* (Springer Science & Business Media, New York).

Au, W. W. L., and Herzing, D. L. (**2003**). "Echolocation signals of wild Atlantic spotted dolphin (*Stenella frontalis*)," J. Acoust. Soc. Am. **113**(1), 598–604.

Azaria, M., and Hertz, D. (**1984**). "Time delay estimation by generalized cross correlation methods," IEEE Trans. Acoust, Speech, Signal Process. **32**(2), 280–285.

Berk, I. M. (**1998**). "Sound production by white shrimp (*Panaeus setiferus*), analysis of another crustacean-like sound from the Gulf of Mexico, and applications for passive sonar in the shrimp industry," J. Shellfish Res. **17**, 1497–1500.

Bertoncini, A., Aguilar-Perera, A., Barreiros, J., Craig, M., Ferreira, B., and Koenig, C. (**2018**). "*Epinephelus itajara* (Atlantic Goliath grouper)," in *The IUCN Red List of Threatened Species* (IUCN, Gland, Switzerland).

Bullock, L. H., Murphy, M. D., Godcharles, M. F., and Mitchell, M. E. (**1992**). "Age, growth, and reproduction of jewfish *Epinephelus itajara* in the eastern Gulf of Mexico," Fish. Bull. **90**(2), 243–249.

Carter, G. C. (**1979**). "Passive ranging errors due to receiving hydrophone position uncertainty," J. Acoust. Soc. Am. **65**(2), 528–530.

Carter, G. C. (**1987**). "Coherence and time delay estimation," Proc. IEEE **75**(2), 236–255.

Cespedes, I., Ophir, J., and Alam, S. K. (**1997**). "The combined effect of signal decorrelation and random noise on the variance of time delay estimation," IEEE Trans. Ultrason, Ferroelect, Freq. Contr. **44**(1), 220–225.

Chérubin, L., and Burgman, R. (**2022**). "Effects of climate change and water management on West Florida Shelf's dynamics," Bull. Mar. Sci. **98**(3), 393–418.

Collins, A. (**2014**). "An investigation into the habitat, behavior and opportunistic feeding strategies of the protected Goliath grouper (*Epinephelus itajara*)," Ph.D. thesis, University of South Florida, Tampa, FL.

Collins, A., Barbieri, L., McBride, R., McCoy, E., and Motta, P. (**2015**). "Reef relief and volume are predictors of Atlantic goliath grouper presence and abundance in the eastern Gulf of Mexico," Bull. Mar. Sci. **91**(4), 399–418.

Coquereau, L., Grall, J., Clavier, J., Jolivet, A., and Chauvaud, L. (**2016**). "Acoustic behaviours of large crustaceans in NE Atlantic coastal habitats," Aquat. Biol. **25**, 151–163.

del Hougne, M., Gigan, S., and del Hougne, P. (**2021**). "Deeply subwavelength localization with reverberation-coded aperture," Phys. Rev. Lett. **127**, 043903.

del Hougne, P. (**2020**). "Robust position sensing with wave fingerprints in dynamic complex propagation environments," Phys. Rev. Res. **2**, 043224.

del Hougne, P., Imani, M. F., Fink, M., Smith, D. R., and Lerosey, G. (**2018**). "Precise localization of multiple noncooperative objects in a disordered cavity by wave front shaping," Phys. Rev. Lett. **121**, 063901.

Duda, R. O., Hart, P. E., and Stork, D. G. (**1973**). *Pattern Classification and Scene Analysis* (Wiley, New York), Vol. 3.

Ferguson, B. (**1989**). "Improved time-delay estimates of underwater acoustic signals using beamforming and prefiltering techniques," IEEE J. Ocean. Eng. **14**(3), 238–244.

Ferguson, B. G., and Lo, K. W. (**2002**). "Passive ranging errors due to multipath distortion of deterministic transient signals with application to the localization of small arms fire," J. Acoust. Soc. Am. **111**(1), 117–128.

Fish, J. F. (**1966**). "Sound production in the American lobster, *Homarus americanus* H. Milne Edwards (*Decapoda reptantia*)," Crustaceana **11**(1), 105–106.

Fish, M. P. (**1964**). "Biological sources of sustained ambient sea noise," in *Marine Bioacoustics*, edited by W. N. Tavolga (Pergamon, New York), Vol. 1, pp. 175–194.

Goold, J. C., and Jones, S. E. (**1995**). "Time and frequency domain characteristics of sperm whale clicks," J. Acoust. Soc. Am. **98**(3), 1279–1291.

Henninger, H. P., and Watson, W. H. III (**2005**). "Mechanisms underlying the production of carapace vibrations and associated waterborne sounds in the American lobster, *Homarus americanus*," J. Exp. Biol. **208**(17), 3421–3429.

Ing, R. K., Quieffin, N., Catheline, S., and Fink, M. (**2005**). "In solid localization of finger impacts using acoustic time-reversal process," Appl. Phys. Lett. **87**(20), 204104.

Iversen, R. T., Perkins, P. J., and Dionne, R. D. (**1963**). "An indication of underwater sound production by squid," Nature **199**, 250–251.

Jain, A. K. (**1989**). *Fundamentals of Digital Image Processing* (Prentice-Hall, Englewood Cliffs, NJ).

Jakuba, M. V., Roman, C. N., Singh, H., Murphy, C., Kunz, C., Willis, C., Sato, T., and Sohn, R. A. (**2008**). "Long-baseline acoustic navigation for under-ice autonomous underwater vehicle operations," J. Field Rob. **25**(11-12), 861–879.

Janik, V. M. (**2000**). "Whistle matching in wild bottlenose dolphins (*Tursiops truncatus*)," Science **289**(5483), 1355–1357.

Johnson, M., Madsen, P. T., Zimmer, W. M. X., de Soto, N. A., and Tyack, P. L. (**2006**). "Foraging Blainville's beaked whales (*Mesoplodon densirostris*) produce distinct click types matched to different phases of echolocation," J. Exp. Biol. **209**(24), 5038–5050.

Jublier, N., Bertucci, F., Kéver, L., Colleye, O., Ballesta, L., Nemeth, R. S., Lecchini, D., Rhodes, K. L., and Parmentier, E. (**2020**). "Passive monitoring of phenological acoustic patterns reveals the sound of the camouflage grouper, *Epinephelus polyphekadion*," Aquat. Conserv: Mar. Freshwater Ecosyst. **30**(1), 42–52.

Kaatz, I. M. (**2002**). "Multiple sound-producing mechanisms in teleost fishes and hypotheses regarding their behavioural significance," Bioacoustics **12**(2-3), 230–233.

Kamminga, C. (**1996**). "Investigations on cetacean sonar XI: Intrinsic comparison of the wave shapes of some members of the phocoenidae family," Aquat. Mamm. **22**(1), 45–55.

Kasumyan, A. O. (**2008**). "Sounds and sound production in fishes," J. Ichthyol. **48**(11), 981–1030.

Kennedy, E., Holderied, M., Mair, J., Guzman, H., and Simpson, S. (**2010**). "Spatial patterns in reef-generated noise relate to habitats and communities: Evidence from a Panamanian case study," J. Exp. Mar. Biol. Ecol. **395**(1), 85–92.

Koenig, C. C., and Coleman, F. (**2013**). "The recovering Goliath grouper population of the southeastern US: Non-consumptive investigations for stock assessment," MARFIN Project (NA10NMF4330123) NOAA/ NMFS Final Report (NOAA, Miami, FL), 70 pp.

Koenig, C. C., Coleman, F. C., and Kingon, K. (**2011**). "Pattern of recovery of the Goliath grouper *Epinephelus itajara* population in the southeastern US," Bull. Mar. Sci. **87**(4), 891–911.

Kunin, V. (**2010**). "Sound and ultrasound source direction of arrival estimation and localization," Ph.D. thesis, Illinois Institute of Technology, Chicago.

Kuroda, M., Miki, N., and Matsuishi, T. F. (**2020**). "Determinants of echolocation click frequency characteristics in small toothed whales: Recent advances from anatomical information," Mammal Rev. **50**(4), 413–425.

Ladich, F. (**2004**). *Sound Production and Acoustic Communication* (Springer Netherlands, Dordrecht), pp. 210–230.

Looby, A., Cox, K., Bravo, S., Rountree, R., Juanes, F., Reynolds, L. K., and Martin, C. W. (**2022**). "A quantitative inventory of global soniferous fish diversity," Rev. Fish Biol. Fish. **32**(2), 581–595.

Madsen, P. T., Carder, D. A., Bedholm, K., and Ridgway, S. H. (**2005**). "Porpoise clicks from a sperm whale nose—Convergent evolution of 130 kHz pulses in toothed whale sonars?," Bioacoustics **15**(2), 195–206.

Malinowski, C., Coleman, F., Koenig, C., Locascio, J., and Murie, D. (**2019**). "Are Atlantic goliath grouper, *Epinephelus itajara*, establishing more northerly spawning sites? Evidence from the northeast Gulf of Mexico," Bull. Mar. Sci. **95**(3), 371–391.

Mann, D., Locascio, J., Coleman, F., and Koenig, C. (**2009**). "Goliath grouper *Epinephelus itajara* sound production and movement patterns on aggregation sites," Endang. Species Res. **7**(3), 229–236.

McDonald, M. A., Hildebrand, J. A., Wiggins, S. M., Johnston, D. W., and Polovina, J. J. (**2009**). "An acoustic survey of beaked whales at cross seamount near Hawaii," J. Acoust. Soc. Am. **125**(2), 624–627.

Moulton, J. M. (**1957**). "Sound production in the spiny lobster *Panulirus argus* (Latreille)," Biol. Bull. **113**(2), 286–295.

Møhl, B., Wahlberg, M., Madsen, P. T., Heerfordt, A., and Lund, A. (**2003**). "The monopulsed nature of sperm whale clicks," J. Acoust. Soc. Am. **114**(2), 1143–1154.

Patek, S. N. (**2002**). "Squeaking with a sliding joint: Mechanics and motor control of sound production in palinurid lobsters," J. Exp. Biol. **205**(16), 2375–2385.

Pinsky, M. L., Selden, R. L., and Kitchel, Z. J. (**2020**). "Climate-driven shifts in marine species ranges: Scaling from organisms to communities," Annu. Rev. Mar. Sci. **12**(1), 153–179.

Radford, C., Stanley, J., Tindle, C., Montgomery, J., and Jeffs, A. (**2010**). "Localised coastal habitats have distinct underwater sound signatures," Mar. Ecol. Prog. Ser. **401**, 21–29.

J. Acoust. Soc. Am. **153** (4), April 2023

Altaher *et al.*   2201

Rountree, R. A., Gilmore, R. G., Goudey, C. A., Hawkins, A. D., Luczkovich, J. J., and Mann, D. A. (**2006**). "Listening to fish," Fisheries **31**(9), 433–446.

Ruppel, C. D., Weber, T. C., Staaterman, E. R., Labak, S. J., and Hart, P. E. (**2022**). "Categorizing active marine acoustic sources based on their potential to affect marine animals," J. Mar. Sci. Eng. **10**(9), 1278.

Sadovy, Y., and Eklund, A. (**1999**). "Synopsis of the biological data on the Nassau grouper, *Epinephelus striatus* (Bloch, 1792) and the jewfish, *E. itajara* (Lichtenstein, 1822)," U.S. Department of Commerce, NOAA Technical Report NMFS 146 and FAO Fisheries Synopsis 157 (Seattle, WA), 65 pp.

Spiesberger, J. L., and Fristrup, K. M. (**1990**). "Passive localization of calling animals and sensing of their acoustic environment using acoustic tomography," Am. Nat. **135**(1), 107–153.

Staaterman, E., Rice, A. N., Mann, D. A., and Paris, C. B. (**2013**). "Soundscapes from a tropical Eastern Pacific reef and a Caribbean Sea reef," Coral Reefs **32**(2), 553–557.

Tavolga, W., Popper, A., and Fay, R. (**1981**). *Proceedings in Life Sciences Hearing and Sound Communication in Fishes* (Springer, New York).

Tyack, P. L. (**1998**). *Acoustic Communication under the Sea* (Springer, Berlin), pp. 163–220.

Van Veen, B., and Buckley, K. (**1988**). "Beamforming: A versatile approach to spatial filtering," IEEE ASSP Mag. **5**(2), 4–24.

Vasconcelos, R. O., Fonseca, P. J., Amorim, M. C. P., and Ladich, F. (**2011**). "Representation of complex vocalizations in the Lusitanian toadfish auditory system: Evidence of fine temporal, frequency and amplitude discrimination," Proc. R. Soc. B **278**(1707), 826–834.

Weisberg, R. H., and He, R. (**2003**). "Local and deep-ocean forcing contributions to anomalous water properties on the West Florida Shelf," J. Geophys. Res. **108**(C6), 3184, https://doi.org/10.1029/2002JC001407

Weisberg, R. H., and Liu, Y. (**2022**). "Local and deep-ocean forcing effects on the west Florida continental shelf circulation and ecology," Front. Mar. Sci. **9**, 863227.

Wiggins, S. M., Frasier, K. E., Elizabeth Henderson, E., and Hildebrand, J. A. (**2013**). "Tracking dolphin whistles using an autonomous acoustic recorder array," J. Acoust. Soc. Am. **133**(6), 3813–3818.

Wozenkraft, J., and Jacobs, I. (**1965**). *Principles of Communication Engineering* (Wiley, New York).

Wu, S. F., and Zhu, N. (**2010**). "Locating arbitrarily time-dependent sound sources in three dimensional space in real time," J. Acoust. Soc. Am. **128**(2), 728–739.

Zeldovich, B. Y., Pilipetsky, N. F., and Shkunov, V. V. (**1985**). *Springer Series in Optical Sciences Principles of Phase Conjugation* (Springer, Berlin).

Zelick, R., Mann, D. A., and Popper, A. N. (**1999**). *Acoustic Communication in Fishes and Frogs* (Springer, New York), pp. 363–411.

Zimmer, W. M. X., Johnson, M. P., Madsen, P. T., and Tyack, P. L. (**2005**). "Echolocation clicks of free-ranging Cuvier's beaked whales (*Ziphius cavirostris*," J. Acoust. Soc. Am. **117**(6), 3919–3927.

Altaher *et al.*